SHAKEDOWN AND DYNAMIC BEHAVIOUR OF MASONRY ARCH RAILWAY BRIDGES

Tamás Forgács[1], Vasilis Sarhosis[2], Sándor Ádány[1]

[1]School of Civil Engineering, University of Leeds, Leeds, LS2 9JT, UK
[2]University of Technology and Economics, H-1111 Budapest, Műegyetem rkp. 3, Hungary

Abstract

Masonry arch bridges form an integral part of our rail infrastructure network and their safety is important for the functioning of our society. Although, there have been several studies to understand the in-service condition of masonry arch bridges, these are mainly focusing on static analyses. However, it is well known that moving vehicles exert a dynamic force on bridges as they cross them. This paper investigates the shakedown and dynamic behaviour of railway masonry arch bridges under traffic load conditions. A nonlinear, mixed discrete-finite element numerical model was developed to investigate static and dynamic response on a masonry arch bridge. Each voussoir of the masonry arch was represented by a distinct block, while the mortar joints were modelled as zero thickness interfaces which can open and close depending on the magnitude and direction of the stresses applied to them. Both static and real dynamic analyses were carried out investigate the effects of moving traffic loads. In addition, investigations into the train to bridge interaction were undertaken and the dynamic amplification factors (DAFs) were estimated. From the evaluation of the results, it was shown that as the external load passes through the bridge, plastic deformations and residual stresses exist in the arch barrel. Also, the dynamic amplification depends on the magnitude of the external load. As the load increases, non-linearity in the structure is evident, which decreases the natural frequency of the bridge. Hence the critical speed is decreasing. Observations provided here reveal new insight into the residual and load carrying capacity of masonry arch bridges.

Keywords: Masonry arch bridge, dynamic analysis, plastic shakedown, moving load, discrete element method, railway bridges

1. Introduction

Europe is sustained by a highly complex and interconnected network of transport infrastructure. Masonry arch bridges forms the backbone of European transport infrastructure network (e.g. there are approximately 200,000 masonry arch bridges still in use on the European railway network [1]) and their reliability and integrity is vital for ensuring economic activity and prosperity. The majority of masonry arch bridges were built in the 19th century, in parallel with the industrial revolution [2]. Today, these are still in-service but showing significant signs of distress. Weathering, demands of increasing axle loads and train velocities [3], plus factors such as increased frequency of flood events due to climate change have introduced extreme uncertainty in the long-term performance of such infrastructure assets. Also, much of our masonry infrastructure has significant heritage and cultural value and in many countries have a policy to "retain and repair", rather than "demolish and replace" them [4]. Failure of such infrastructure could lead to direct and indirect costs to the economy and society and hamper rescue and recovery efforts. From the above, there is an imperative need to better understand the mechanical behaviour of masonry arch bridges and provide detailed and accurate data that will better inform maintenance programmes and asset management decisions. Without a strategic approach to caring for our ageing masonry infrastructure, we run the risk of over-investing in some areas while neglecting others that are in need of our attention.

However, assessing the structural performance of ageing masonry infrastructure is a complex task. Previous research has clearly demonstrated that the assessment methods currently used by the industry are antiquated and/or over-simplistic. For example, for the assessment of masonry arch bridges, the Military Engineering Experimental Establishment (MEXE) method of assessment is still in use especially in UK. This is a semi-empirical approach based on an elastic analysis by Pippard et al. [5] who modelled the arch barrel as linear elastic, segmental in shape, pinned at its support and carrying a central point load. The method dates back to the 1940s, has very limited predictive capability, and offers little scope for future enhancement [6]. Other assessment approaches used by the industry (particularly in the UK) are: a) the static theorem of plastic limit analysis (developed into the Archie-M software) which uses simple equilibrium calculations (the self-weigh of the arch barrel and live loads are balanced by forces between the blocks); and b) the RING software which is based on the rigid block theory and uses the kinematic theorem of limit analysis to identify the collapse state with the smallest external loading and hence predict the ultimate load [7]. Although the primary focus of these methods has been on the prediction of structural failure of ageing masonry infrastructure, prediction of the service load above which incremental damage occurs is now a key priority for infrastructure owners, who are under increasing pressure to provide transport networks which are secure and resilient [8].

Over the last three decades, significant efforts have been devoted to the development of numerical models to represent the complex and non-linear in-service behaviour and limit state capacity of masonry structures subjected to external loads. Such models range from considering masonry as a continuum (macro-models) to the more detailed ones that consider masonry as an assemblage of units and mortar joints (micro-models/meso-scale models); see Boothby [9] and Sarhosis et al. [10]. In particular, Choo and Gong [11] have successfully used the Finite Element Method (FEM) to developed models of masonry arch bridges to predict their ultimate load carrying capacity. However, in macro-models based on the FEM, the description of the discontinuity is limited since they consider the arch as a continuum element [10, 12]. An overview of such models can be found in Boothby [13] and Sarhosis et al. [10]. Given the importance of the masonry unit-to-mortar interface [14, 15] on the structural behaviour of aged masonry arch bridges, micro-modelling approaches (i.e. those based on Discrete-Finite Element Method) are better suited to simulating their serviceability and load carrying capacity [16-18]. Sophisticated FEM approaches (e.g. those based on the contact element techniques) were able to reflect the discrete nature of masonry e.g. those presented by Fanning and Boothby [9], Gago et al. [19], Ford et al. [20] and Drosopoulos et al. [21]. However, such methods require high computational cost, are unable to realistically predict the crack development at serviceability limit state and have convergence difficulties when blocks fall or slide excessively. Another modelling approach is the one described by the fibre-beam approach which can predict the collapse mechanism of masonry and to account for the effective material behaviour with acceptable computational effort. According to the method, the masonry arch can be modelled as a segmental fibre-beam [22]. The approach has been successfully used to study the behaviour of masonry arches and arch bridges under static and dynamic conditions [23]. Despite the simplifications in the representation of structural geometry, it was found a promising approach for preliminary assessment of the seismic capacity of masonry arch bridges.

An alternative and attractive method in which the discrete nature of the masonry can be more realistically represented is the Discrete Element Method (DEM). The advantage of the DEM is that it considers the arch as a collection of separate voussoirs able to slide and rotate relative to each other. The DEM was developed by Cundall [24] to model blocky-rock systems and sliding along rock mass. The approach was recently implemented to simulate the mechanical response of masonry structures including arches [14, 16, 25-27] in which failure occurs along mortar joints. From past studies carried out using DEM to simulate the mechanical response of masonry arch bridges, it was found that the method is suitable and reliable especially in the case in which failure is dominated at masonry unit-to-mortar interface [12]. Also, an important finding from past literature review studies presented by Sarhosis et al. [10] is that the majority, if not all, of the past research is focusing on the behaviour of masonry arch bridges subjected to static loads. In such studies, to reach conclusions related to the load carrying capacity of masonry arch bridges, an increasing in magnitude point load is applied at the quarter and/or at mid-span of the masonry arch bridge.

However, vehicles crossing masonry arch bridges are exerting dynamic loads on them. Most of the standards and industry guidelines [1, 3, 28, 29] suggest the use of dynamic amplification factors to take into account such effects. In this case, static analysis can be carried out, while the static response of the structure (e.g. displacements, internal forces, stresses) should be multiplied by the dynamic amplification factor. In this way, real dynamic analysis can be avoided. Also, there are several analytical [30], numerical [31-34] and experimental [35] studies investigating the dynamic response of masonry arch bridges. Smith and Acikgoz [30] investigated the dynamic behaviour of linear elastic curved beams. Partial differential equations of the vibration were derived and solved numerically. Dynamic amplification factors were determined. According to the authors, codified procedures can significantly underestimate the dynamic amplification. In addition, Ataei at al. [35] estimated the dynamic amplification factors of eleven multi-span masonry arch bridges. Vertical deflection of the crown was measured when different in speed and weight train crossed the bridge. Moreover, due to the importance of this subject, many guidelines are provided by various codes and design standards (e.g ERRI-D214 [36]) for designing and performance assessment on the dynamic characteristics of bridges. However, from the above studies it is evident that assessing the in-service condition of masonry arch bridges is a rather difficult task. This is mainly due to the complexity of the problem and that recent studies have reported contradictory results.

This paper aims to study the dynamic phenomena on masonry arch bridges due to vehicle load. A numerical model has been developed to analyse both static and dynamic response of masonry arch bridges with the purpose of estimating the traffic effects by means of moving loads. As a case study, the geometrical characteristics of the Prestwood bridge have been adopted in the investigations. The structural assessment and numerical analyses of the bridge were performed based on a detailed finite-discrete element code. Suitable constitutive laws were considered for the mortar joints and for the backfill. The numerical results were compared against field test results. The interaction between the train and the track is considered through a simplified methodology. Two different types of static analyses (incrementally increased load at fixed points and quasi-static moving load) and real dynamic analysis were carried out. In addition, dynamic amplification factors (DAFs) were estimated. Results of this study were used to assess how train load and train speed affect the DAF on a masonry arch bridge.

2. Current dynamic amplification factors for railway bridges

The passage of trains on bridges exerts dynamic effects on them. Dynamic effects are able to change the structural response (e.g. the displacements, internal forces etc.) of a bridge. According to Eurocode [28], the extent of the dynamic effects on bridges depends mainly on: a) the velocity of the train; b) the number and weights of the axles; c) the span of the bridge; and d) the natural frequency (mass and stiffness) of the bridge. Other factors which may influence the dynamic effect in bridges are the railway track to train interaction and the dynamic characteristics of the ballast; but these effects are out of scope of this work. The simplified method of Eurocode (EN 1991-2:2003) for railway bridges enables the engineer to carry out static analysis with LM71 vertical load model and multiply the structural response with the dynamic amplification factors calculated as:

$$\Phi_2 = \frac{1.44}{\sqrt{L_\phi} - 0.2} + 0.82 \qquad 1.00 \le \Phi_2 \le 1.67\,, \tag{1}$$

$$\Phi_3 = \frac{2.16}{\sqrt{L_\phi} - 0.2} + 0.73 \qquad 1.00 \le \Phi_3 \le 2.00\,, \tag{2}$$

where L_ϕ is the determinant length in meters (see EN 1991-2: Traffic load on structures), while Φ_2 and Φ_3 are the dynamic factors for carefully maintained tracks and tracks with standard maintenance, respectively. These formulas can only be used if: a) the first natural frequency of the structure does not exceeds the lower and upper-limit for natural frequency defined in the standard; and b) the train velocity does not exceed 200 km/h (56 m/s). It should be noted that the dynamic amplification of EN 1991-2 simplified method does not depend on the velocity of the train.

EN 1991-2 Annex C [28], Network Rail [29] and UIC suggest another method to calculate the dynamic amplification factor (Eq. (3) and (4)). This method takes into account not just the span and the first natural frequency of the structure, but the velocity of the train as well. The dynamic enhancement can be calculated as:

$$\varphi' = \frac{K}{1 - K + K^4} \tag{3}$$

$$K = \frac{v_x}{2 n_0 L_\phi} \tag{4}$$

where v_x is the velocity of the train in meters per second, L_ϕ is the determinant length in meters and n_0 the first natural frequency of the bridge in Hz. Equations (3) and (4) were determined in the 60's to conservatively characterize the dynamic response of simple supported concrete and steel bridges [37]. To handle the different mode shapes of the different structural systems, determinant length (L_ϕ) was introduced. In the case of single span arch bridges, the determinant length should be the half of the span. In Figure 1, the DAF were calculated for a 6.55 m single span arch bridge with various natural frequencies according to Eqs (3) and (4).

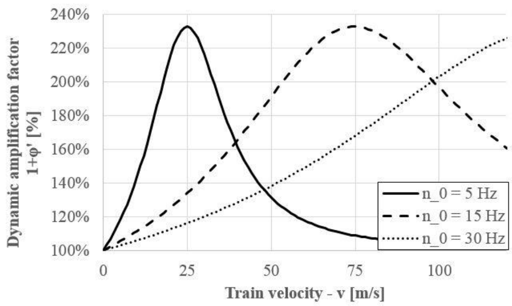

Figure 1 – Dynamic Amplification Factor according to Network Rail [29]

3. The proposed mixed discrete-continuum approach to evaluate the dynamic response of masonry arch bridges

Understanding the mechanical behaviour of masonry arch bridges is a challenging task for an engineer. Even under static conditions, the mechanical behaviour of masonry arch bridges is complex and the analytical tools available by engineers to assess the life expectancy of such bridges needs refinement. The selection of the most appropriate computational method to use for the analysis of masonry structures, among other factors, should include representation of joint opening between voussoirs in the arch; sliding between the arch barrel and the soil, plastic response in the backfill above the arch etc. In case of dynamic analysis, in addition to the aforementioned factors, the computational model should include inertial and vehicle-structure interaction effects.

To computationally evaluate the dynamic response of masonry arch bridges, the mixed discrete-continuum element code UDEC, developed by ITASCA has been used in this study. Within UDEC, voussoirs in the barrel vault were represented by distinct linear-elastic deformable blocks separated by zero thickness interfaces at each mortar joint. The voussoirs were subdivided into finite elements so that stresses can be calculated. Backfill was represented as a linear elastic-perfectly plastic material. Deformability and non-linear behaviour of backfill was approximated with finite element discretization. The model makes use of an explicit dynamic solution scheme, which makes it able to carry out real dynamic analysis.

3.1. Contact formulation and solution procedure

The discrete elements can interact with each other through zero-thickness interface elements. At the interfaces, blocks are connected kinematically to each other by sets of point contacts [38, 39], along the outside perimeter of the blocks, at locations where corners or edges meet [16]. In the model, large block movements are allowed, including cases of complete detachment and re-closure when external forces are applied to them, with no attempt to obtain a continuous stress distribution through the contact surface.

At each contact point, there are two spring connections. These can transfer either a normal force or a shear force from one block to the other. In the normal direction, the mechanical behaviour of the joints (i.e. the zero-thickness contact interface) is governed by the following equation (Figure 2a):

$$\Delta\sigma_n = k_n \Delta u_n , \qquad (5)$$

where k_n is the normal stiffness of the contact and Δu_n is the increment in normal contact displacement, i.e., the relative displacement between the blocks at the contact point. Similarly, in the shear direction, the mechanical behaviour is controlled by the constant shear stiffness k_s using the following expression (Figure 2b):

$$\Delta\tau_s = k_s \Delta u_s , \qquad (6)$$

where $\Delta\tau_s$ is the change in shear stress, and Δu_s is the increment in shear displacement.

In the present research work, the contacts are assumed to follow the Mohr-Coulomb failure criterion, commonly used to represent shear failure in soils and rocks. The criterion has a limiting tensile strength, f_t. If the contact normal stress exceeds the tensile strength, then the normal stress is set to zero and the interface opens. Alternatively, at those contacts undergoing compression, a small overlap will occur between block edges (Figure 2a). The amount of overlap is controlled by the normal stiffness. Similarly, in shear, in the elastic range, the response is controlled by contact shear stiffness (Figure 2b). In addition, in the shear direction, slippage between blocks occurs when the tangential or shear stress at a contact exceeds a critical value τ_{max} defined by:

$$\left|\tau_s\right| \leq c + \sigma_n \tan\left(\varphi\right) = \tau_{\max} \,, \qquad (7)$$

where $\mu = \tan\left(\varphi\right)$ is the friction coefficient and φ the angle of friction and c the cohesive strength. After slip takes place, the shear stress is reduced according to the Mohr-Coulomb criterion, but using residual values for cohesion (c_{res}) and friction (φ_{res}), as shown in Figure 2b. Non-associative flow rule is applied therefore the dilation angle (ψ) is set to zero. After a contact breaks or slips, forces are redistributed, and it might cause adjacent contacts to break.

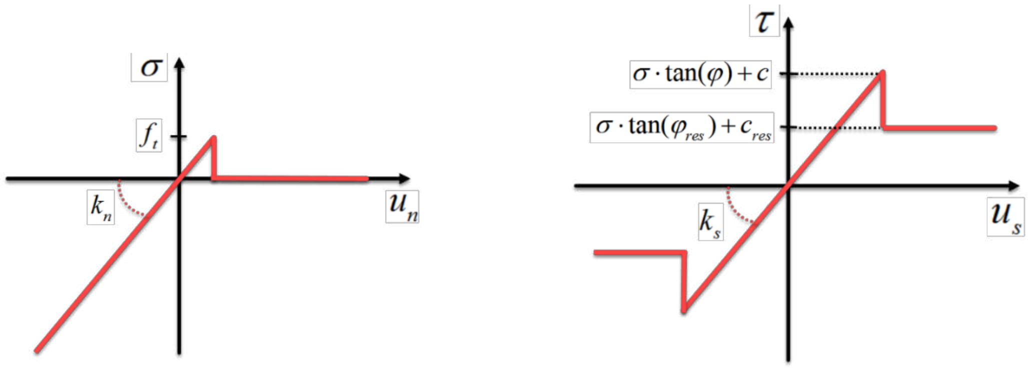

(a) (b)

Figure 2 –Mechanical behaviour of contacts in (a) normal and in (b) shear direction

In the presented model, the Newtonian equations of motion are solved directly by the UDEC with an explicit time stepping algorithm. The explicit scheme applies the central difference method. As a result, velocity of each node can be calculated. With the help of nodal velocities, displacements and location of the nodes can be updated. After the new position of the elements is known, contact locations and orientation can be calculated. Contact forces are updated by invoking the contact constitutive law, as described in the previous section. For the internal finite elements, nodal displacements lead to new strains, from which zone stresses ensue by applying the assumed material constitutive model. In this way, nodal forces can be assembled for the next calculation step.

The central difference method is only conditionally stable. To avoid numerical instabilities arising from calculation of block deformation, a limiting timestep is evaluated for each node. This limiting timestep is depend on the mass associated with block node; the elastic properties of the block material and the size of the finite element. Moreover, another limiting timestep for the inter-block relative displacement should be calculated and it depends on the mass of the smallest block and the maximum contact stiffness in the system. The geometry of the finite elements can change during the mechanical process, hence the controlling timestep for the analysis needs to be recalculated in every calculation step.

In the case of static analysis, artificial damping is applied to reach equilibrium as fast as possible. Here the role of the damping is a numerical servo-mechanism to absorb the unwanted elastic oscillations of the system. While in the case of dynamic simulation, the role of the damping is to model the energy loss of materials. Energy absorption can develop in plastic material behaviour and with frictional sliding as well. During dynamic simulations, additional Rayleigh damping was not applied.

3.2. Vehicle-structure interaction

Vehicle-structure interaction was implemented into UDEC via FISH programming (embedded programme language of Itasca software) as a single degree of freedom system (see Figure 3). The differential equation of the vehicle's motion can be written as:

$$m\ddot{y}(t) + \alpha(t)\left[c\left(\dot{y}(t) - \dot{u}(t)\right) + k\left(y(t) - u(t)\right)\right] = mg \,, \qquad (8)$$

where m is the mass of the vehicle. Spring stiffness and damping coefficient was obtained from [31]: $k = 159500$ N/m and $c = 0.2 \times 2\sqrt{k \times m}$, respectively. $y(t), \dot{y}(t), \ddot{y}(t)$ are the vertical displacement, velocity and the acceleration of the vehicle, while $u(t), \dot{u}(t)$ are the vertical displacement, and velocity of the track. $\alpha(t)$ is intended to represent the possibility of detachment between the vehicle and the track as follows:

$$\alpha(t) = \begin{cases} 0 & \text{if} \quad k\left(y(t) - u(t)\right) + c\left(\dot{y}(t) - \dot{u}(t)\right) \geq 0 \\ 1 & \text{if} \quad k\left(y(t) - u(t)\right) + c\left(\dot{y}(t) - \dot{u}(t)\right) < 0 \end{cases}, \tag{9}$$

From Equation (9), if the force between the vehicle and the track is in tension, then the differential equation is reduced to the differential equation of free fall, while the contact force is set to zero.

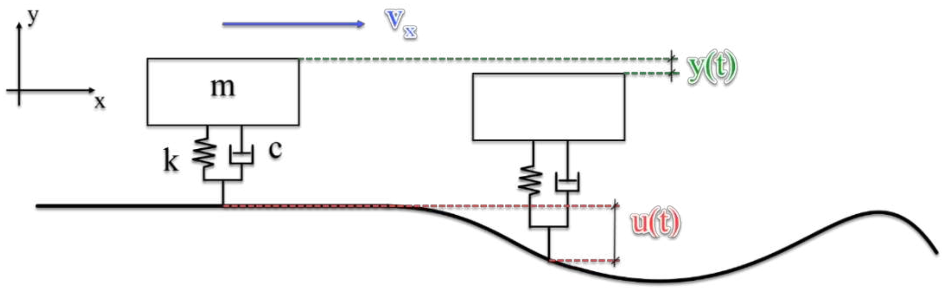

Figure 3 – Single degree of freedom mass-spring-damper model for vehicle-structure interaction

The ordinary differential equation described in Equation (8) is solved numerically with the forward Euler method. The initial conditions are:

$$\begin{aligned} y(0) &= \frac{-mg}{k} \qquad & u(0) &= 0 \\ \dot{y}(0) &= 0 \qquad & \dot{u}(0) &= 0 \end{aligned}. \tag{10}$$

The timestep used during solution is equal to the critical timestep determined by UDEC for solution. The vertical displacement and the velocity of the vehicle are calculated with Equation (11) and (12), respectively. This calculation process was done simultaneously with the built-in UDEC solution algorithm applying the same timestep.

$$y(t) = y(t - \Delta t) + \dot{y}(t - \Delta t)\Delta t \ , \tag{11}$$

$$\dot{y}(t) = \dot{y}(t - \Delta t) + \alpha(t - \Delta t)\left(\frac{mg - c\left(\dot{y}(t - \Delta t) - \dot{u}(t - \Delta t)\right) - k\left(y(t - \Delta t) - u(t - \Delta t)\right)}{m}\right)\Delta t \ . \tag{12}$$

4. Development of the numerical model

Although several research, including the one from the authors of this manuscript [40, 41], have been done in the past to computationally model and understand the three dimensional mechanical behaviour of masonry arch bridges, the work presented herein uses a 2D mixed discrete-finite element approach. The reason for adopting a 2D model in this study was to understand better the basic nature of the investigated phenomena, while the released computational needs enables the authors to use more accurate (more dense) finite element mesh, and more parametric studies to be carry out in a computationally efficient manner. By using a 2D model, the possibility to analyse transverse behaviour (e.g. effect of spandrel walls, transverse load distribution) is dismissed. Moreover, other elements of a railway bridge like ballast, sleepers and rail were neglected in the model.

4.1. Geometry and materials used for the development of the numerical model

The geometry and material properties of the investigated structure was taken to represent the Prestwood Bridge, UK. There was no intention to model the foundations and the subsoils in detail. Page [42] carried out full scale experimental tests on Prestwood Bridge to determine the load bearing capacity of the structure. The validation of the adopted model against the field scale results is presented in [39]. Details of the geometry of the model are shown in Figure 4 and in Table 1.

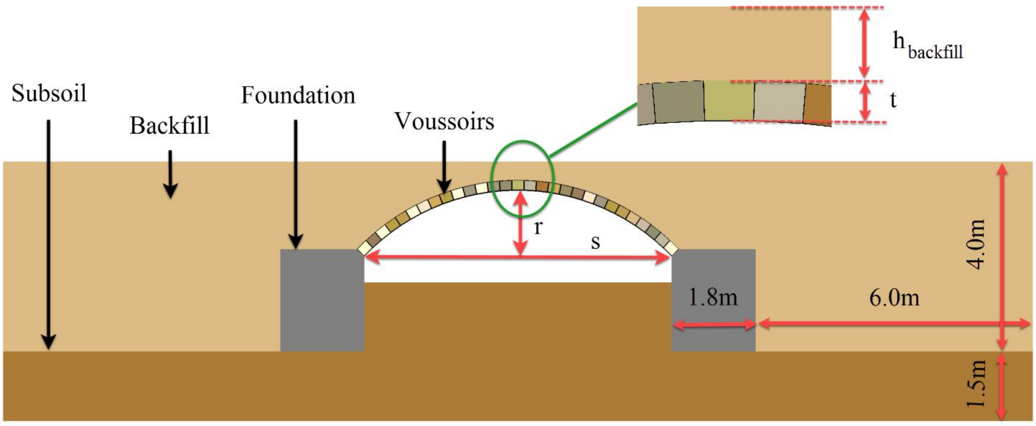

Figure 4 – Geometrical characteristic of the numerical model

Table 1 – Geometrical characteristic of the bridge

Span	**Rise**	**Barrel thickness**	**Height of the backfill**
6.550 m	1.428 m	0.220 m	0.400 m

The foundation of the bridge and the voussoirs of the arch ring were assumed to behave in a linear elastic manner. The backfill of the arch bridge was simulated as linear elastic-perfectly plastic material, according to Mohr-Coulomb failure criterion. Material properties of typical limestone were used for the voussoirs. In addition, well-compacted sandy gravel were applied as backfill material. The material parameters were summarized in Table 2. Although geotechnical materials show significant variability, there was no intention to incorporate this effect in the present paper. Mortar joints between voussoirs were represented as zero thickness interfaces. In this study, considering that we are dealing with ageing low bond strength masonry, the tensile and cohesive resistance of the mortar was neglected and assumed equal to zero. Only frictional sliding between the voussoirs was allowed to occur. Similarly, only frictional resistance was allowed at the interface between the voussoirs and the backfill material. Table 3 shows the material properties used for the development of the contact model. Contact normal stiffness was chosen sufficiently high value to avoid significant interpenetration between the elements. Friction angles between voussoirs and for the voussoir-soil interface were chosen according to guidelines [3].

Table 2 – Material parameters used in the numerical model.

Material	Density	Young modulus	Poisson's ratio	Friction angle	Cohesion	Tensile strength
Voussoirs	2500 kg/m^3	20 GPa	0.20	-	-	-
Foundation	2500 kg/m^3	20 GPa	0.20	-	-	-
Backfill	2000 kg/m^3	0.20 GPa	0.25	37°	5 kPa	5 kPa
Subsoil	2000 kg/m^3	5 GPa	0.25	50°	500 kPa	500 kPa

Table 3 – Contact parameters at the interfaces

Contact location	Contact stiffness	Friction angle
Voussoir to voussoir	100 GPa/m	40°
Backfill to arch barrel	100 GPa/m	20°
Backfill to subsoil	100 GPa/m	20°

4.2. Finite Element discretization and boundary conditions

UDEC is using a constant-strain triangular finite elements by default. These elements can behave excessively stiff in plane-strain problems where plastic failure occurs. Plane-strain geometries can introduce a kinematic restrain in the out of plane direction, often giving rise to overprediction of the collapse load. To eliminate the non-physical hourglass modes of deformation, a discretization scheme proposed by Marti and Cundall [43] was used. In the applied discretization scheme, the discretization for the isotropic part of the strain and stress tensors differs from the discretization for the deviatoric part.

Moreover, to obtain accurate stress distribution in the voussoirs, a detailed discretization of the voussoirs implemented. In particular, the number of point contacts between the voussoirs was set high to ensure the accurate calculation of contact stresses. Convergence tests were carried out on the model to determine the appropriate number of finite elements for the voussoirs and for the backfill (Figure 5a). As a result, every voussoir was divided into 8×8×4 finite elements (Figure 5b), while the density of the FE mesh for backfill was assigned to be more dense above the crown (i.e. edge length ~5 cm) and coarser towards the sides of the model (i.e. edge length ~20 cm). The applied discretization is marked with red colour in Figure 5a.

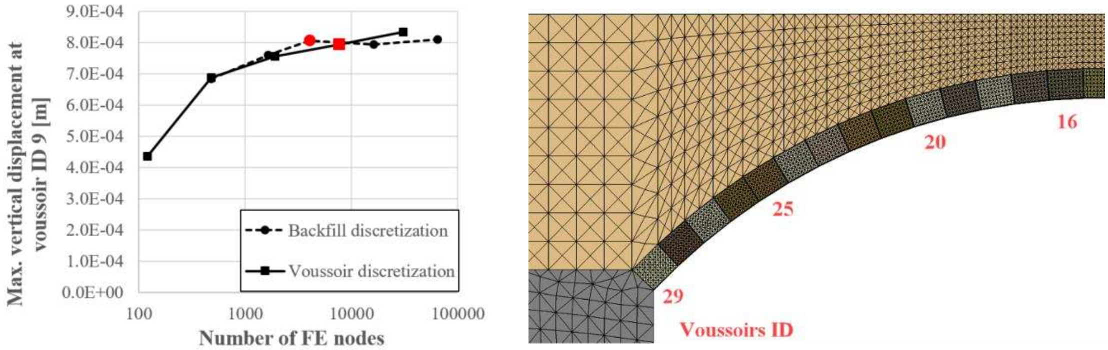

(a) (b)

Figure 5 – Finite element mesh for voussoirs and for backfill used for the development of the numerical model

On the external boundaries, the velocity of the finite element nodes was set to zero. The boundaries of the model were defined sufficiently far from the structure to avoid the reflection of stresses from the boundaries during dynamic simulations. Moreover, non-reflecting viscous boundary was applied at the boundaries of the model.

The present paper neglects the presence of the track. In reality, it can be assumed that the train transmits its concentrated loads to the rail. These loads are dispersed by the sleepers and the ballast. It is assumed that the load is distributed on a $d_{load} = 1.0$ m loaded length. Triangular distribution was selected to ensure numerical stability (Figure 6).

The maximum intensity of distributed load was calculated using the equation below:

$$p_{\max} = \frac{2R_y}{d_{load}}, \tag{13}$$

where R_y is the resultant of the external load, d_{load} is the length where the resultant force was distributed.

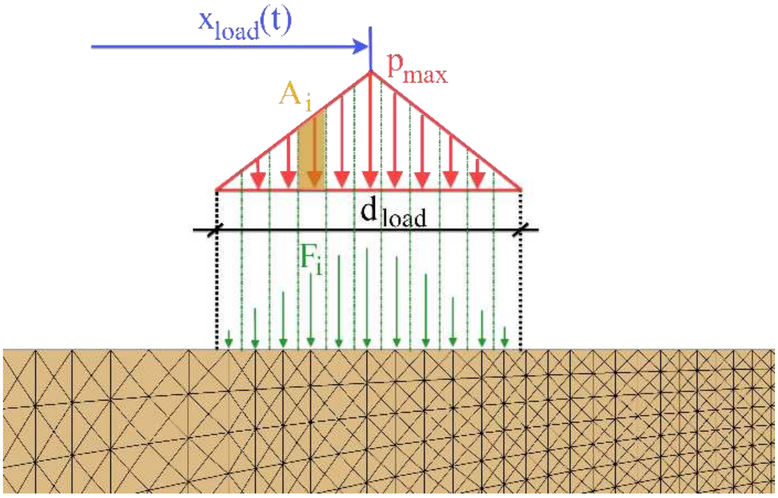

Figure 6 – Distribution of the external load

4.3. Types of analysis performed

Both static and dynamic analysis were carried out. The aim of dynamic analysis was to determine the dynamic response of the bridge. Moreover, investigations on the effect of magnitude of the external load on the dynamic amplification were made. In every simulation, as an initial step, the self-weight of the structure was assigned and equilibrated. Criterion for equilibrium was defined as the ratio of the average unbalanced mechanical force magnitude divided by the average applied mechanical force magnitude for all grid-points in the model. When this ratio was lower than 1.0e-6, the structure was considered to be in equilibrium. At this stage, nodal velocities typically lower than 2.0e-6 m/s. Near to the state of failure, convergence of the numerical model decreases significantly. Therefore, another limit was introduced as: *if the state of equilibrium cannot be reached within 300,000 calculation cycles in a single loading step, then the simulation was stopped and the corresponding load was considered as the failure load.*

4.3.1. Incrementally increased load at fixed positions along the span of the bridge (Type 1)

Experimental and field tests carried out on full-scale masonry arch bridges are typically using vertical loads at quarter span to gain information about the structural stiffness and load bearing capacity. The advantage of using numerical simulations is that models can be developed in which parametric studies can be carried out e.g. load can be applied in several loading positions in the bridge. In this study, numerical models have been carried out in which the load position has been varied along the span of the bridge. The procedure was as follows (Figure 7b): After a fixed x/s load position was selected (in which x is the distance from the edge of the arch ring of the bridge and s is the span of the bridge); the distribution of the load was defined according to Figure 6, while the magnitude of the vertical load was incrementally increased (i.e. load increment: 1.0 kN/m) until the structure failed. The simulation was repeated in nine different loading positions, i.e. from $x/s = 0.0$ until $x/s = 8/16$. In this way, load bearing capacity versus load position were plotted. The global minimum in the load bearing capacity versus the load position relationship can be considered as the load bearing capacity of the bridge. The flowchart for this type of simulation can be seen in Figure 7a.

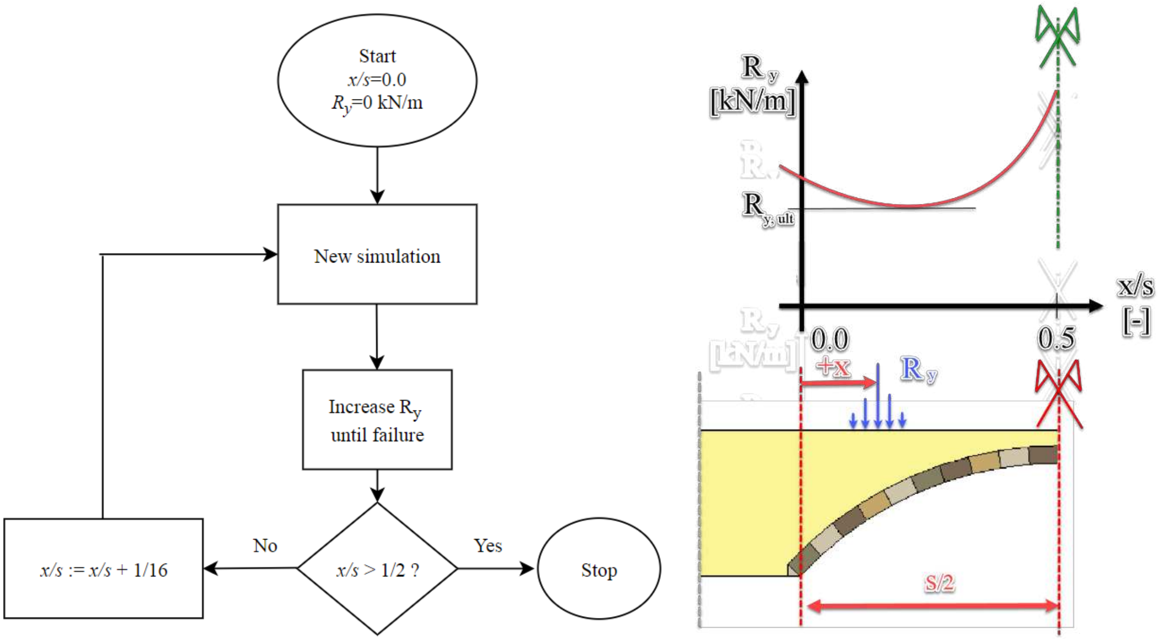

(a) (b)

Figure 7 – Flowchart for incrementally increased load at fixed positions (Type 1)

4.3.2. Quasi-static moving load along the span of the bridge (Type 2)

It is believed that in the numerical model, the movement of a train axle might be better represented if the magnitude of the external load is kept constant while the position of the load is changing step-by-step, as the load is passing through the bridge. The load model defined in Section 4.2 (Equation 16) was applied in this case as well. After the structure reached the equilibrium, the load was moved by 0.10 m. If the load could cross the bridge without causing failure of the structure, the external load magnitude was increased. If the structure reaches its ultimate state (i.e. failure) during simulation, a new simulation was started with a decreased load magnitude. The simulations were repeated until the load bearing capacity of the structure was determined with sufficient precision (+/- 1.0 kN/m). Figure 8 shows the flowchart for this type of simulation.

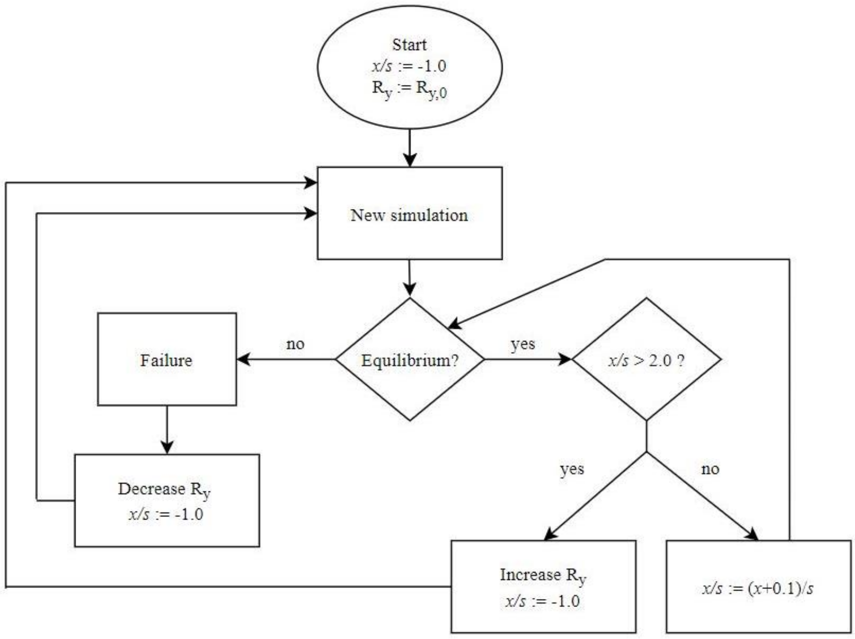

Figure 8 – Flowchart for quasi-static moving load analysis (Type 2)

4.3.3. Dynamic analysis (Type 3)

During the dynamic analysis the artificial damping and mass scaling were not applied during simulations. Energy dissipation can develop within the model via frictional sliding (e.g. at the extrados of the arch barrel where backfill can slide upon the voussoirs) or via the plastic deformations of the backfill material. As a conservative assumption, Rayleigh damping was not applied during the analysis. The external load was dragged through on the bridge with constant horizontal velocity (investigated range was between 10 to 120 m/s). Simulations were ended when: (i) the external load could cross the bridge and reached $x/s = 1.60$ without causing failure; or (ii) during the simulation the bridge failed. These simulations were repeated with different magnitude of external load.

During the analysis, radial displacements of each voussoir, maximal contact stresses at the inner and the outer side of the bed joints were recorded and plotted against the position of the external load. Dynamic response of the structure was compared to the static response and dynamic amplification factors obtained. Two types of dynamic amplification factor was evaluated. These are: (a) global dynamic amplification factor (DAF_{global}) , where the highest dynamic response of the structure was selected and compared with the highest static response; and (b) local dynamic amplification ($DAF_{local,i}$) was defined for every voussoir as the highest dynamic response of the selected element compared to the static response of the same element:

$$DAF_{global} = \frac{\max_i \left| y_{dyn,i,\max} \right|}{\max_j \left| y_{stat,j,\max} \right|} \qquad i, j = \{1 \ldots \text{number of voussoirs}\}, \tag{14}$$

$$DAF_{local,i} = \frac{\left| y_{dyn,i,\max} \right|}{\left| y_{stat,i,\max} \right|} \qquad i = \{1 \ldots \text{number of voussoirs}\}, \tag{15}$$

where $y_{dyn,i,\max}$ is the maximal dynamic and $y_{stat,i,\max}$ is the maximal static response of the i^{th} element in a single simulation, respectively.

5. Results

5.1. Results of the static analysis (Type 1 and 2)

To get a first impression of the structural behaviour of the masonry arch bridge under investigation, the failure load under static conditions was determined. With respect to the load bearing capacity, Type 2 analysis of moving load showed lower ultimate load by 7% (~71 kN/m) compared to Type 1 analysis (~76 kN/m). The difference might be attributed partly due to the precision of the loading procedure, i.e. the load increment was 1.0 kN/m; which can cause +/-1.5% error difference. Moreover, in the case of quasi-static moving load, the load path/load history could cause weaker behaviour by non-elastic deformation of the system. Type 2 simulation at ultimate load stopped at $x/s = 0.14$, which is close to the critical position obtained from Type 1 simulation ($x/s = 0.125$).

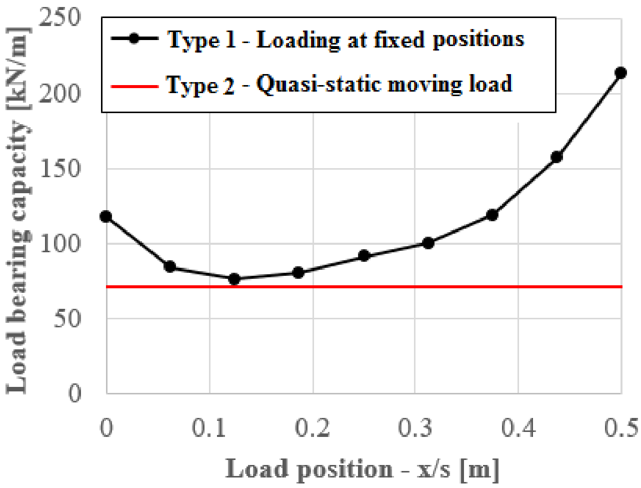

Figure 9 – Ultimate load bearing capacity of the bridge

With respect to Type 1 analysis, load-deflection curves were obtained. Such analyses can be used to determine the stiffness of the bridge. On the other hand, Type 2 analysis can provide valuable information about the response (e.g. stresses, displacements) of the structure when the load of the vehicle is passing from the bridge. Figure 10a-c shows the influence lines for radial displacements and contact normal stresses at ¾ span of the bridge. With the increasing magnitude of external loads, contacts can open (the normal stress decreases to 0 MPa) and close. Maximum contact stresses from influence lines in Figure 10b-c were plotted against the ratio of external load magnitude divided by the ultimate load (Figure 11). It was found that the maximum of the contact stress increases exponentially as the load increases.

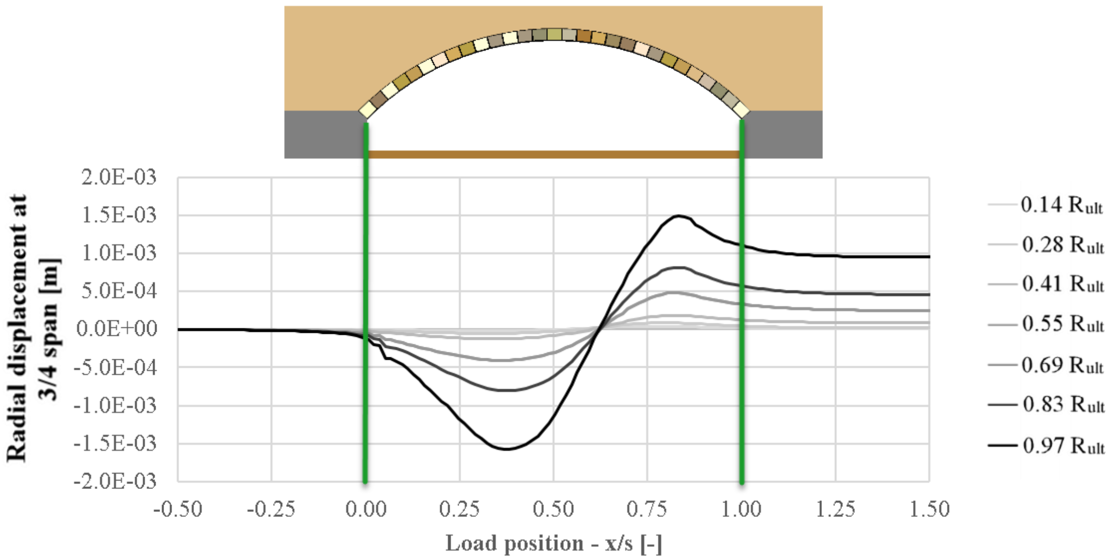

(a)

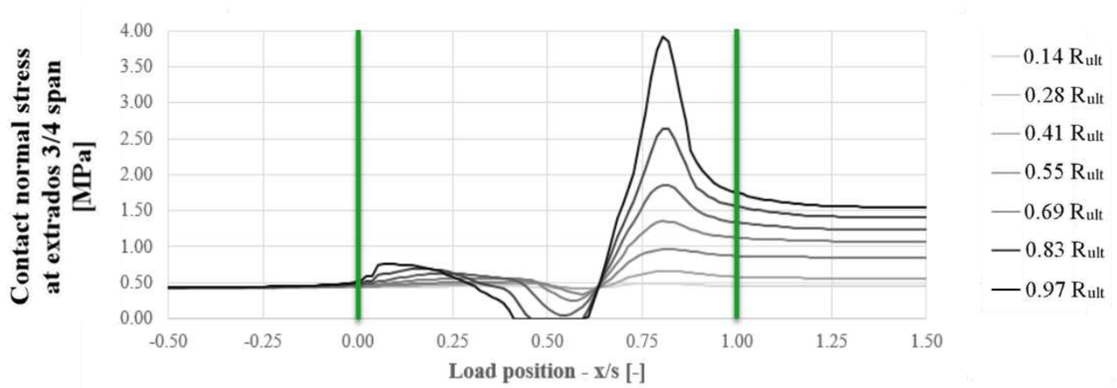

(b)

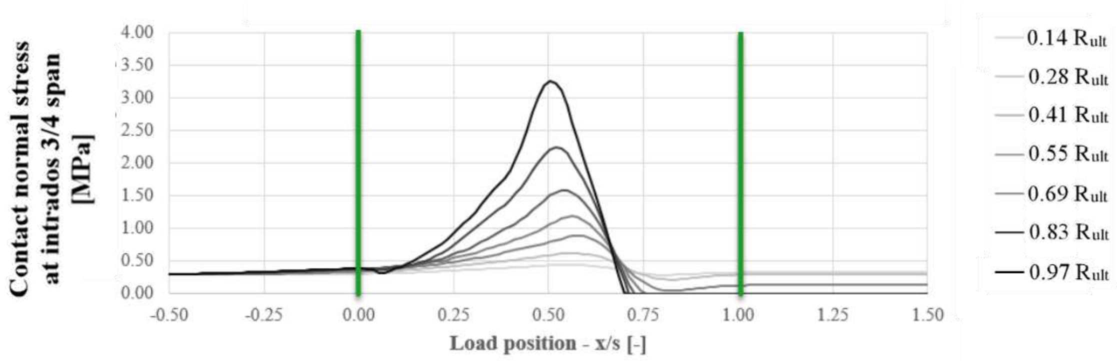

(c)

Figure 10 - Influence lines for voussoir at ¾ span: (a) radial displacements; (b) contact stresses extrados side and (c) contact stresses at intrados side (Type 2 analysis)

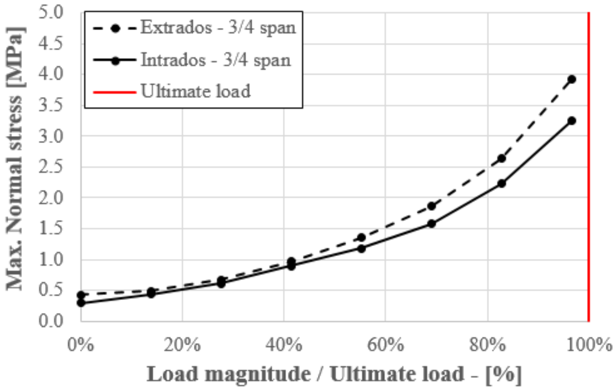

Figure 11 – Maximum contact normal stress at ¾ span.

After the axle load passed through the bridge, the stresses within the structure went through redistribution: e.g. at $0.55R_{ult}$ (40 kN/m) and above a crack appeared (normal stress decreased to 0 Pa) and remained open at ¾ span intrados after the load left the bridge. Figure 12 represents the residual stress state of the arch barrel and the backfill after one cycle of external load passed through the structure when loaded under a quasi-static manner. The residual stress state depends on the magnitude of the external load. The arch barrel of the "*never loaded*" structure shows uniform normal stress distribution and the stresses between the voussoirs of the arch are in compression. As the magnitude of the external load increases, the residual stress state of arch barrel contains significant bending as well.

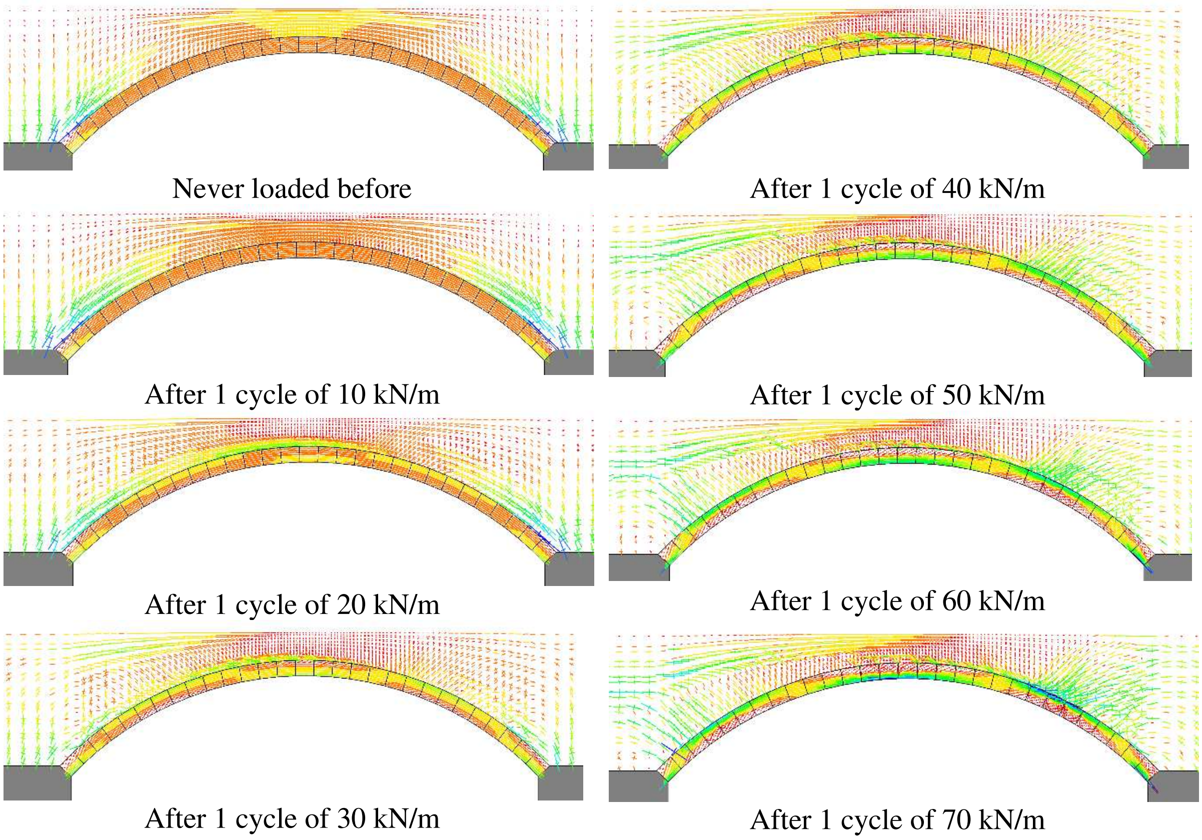

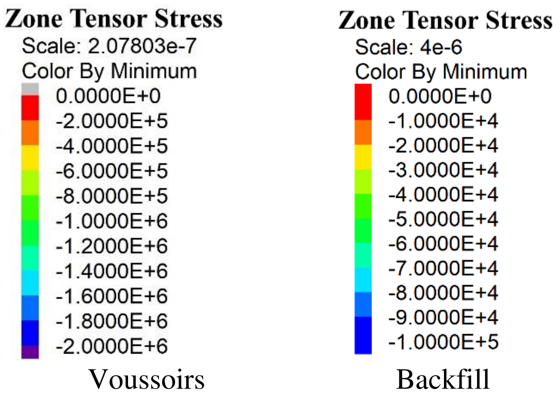

Figure 12 – Residual stress state after one cycle of external load crossed the structure (negative values mean compression – Type 2 analysis)

Axle loads follow each other simultaneously and trains would cross the bridge typically in both directions (i.e. left to right and right to left). Figure 13 shows the normal stresses at ¾ span (extrados side), while the axle load (R_y = 30 kN/m = $0.42R_{ult}$) crossed the bridge 10 times. The distance between the loads was chosen sufficiently large to avoid interaction between the loads). According to Figure 13, after the third cycle, additional redistribution of the stresses cannot be observed. Also, when the moving load is in backward direction, we have redistribution of stresses and maximum displacement occurs at different load position, see Figure 14a. Convergence to the shakedown state was slower in case of two directional and faster in case of one directional loading.

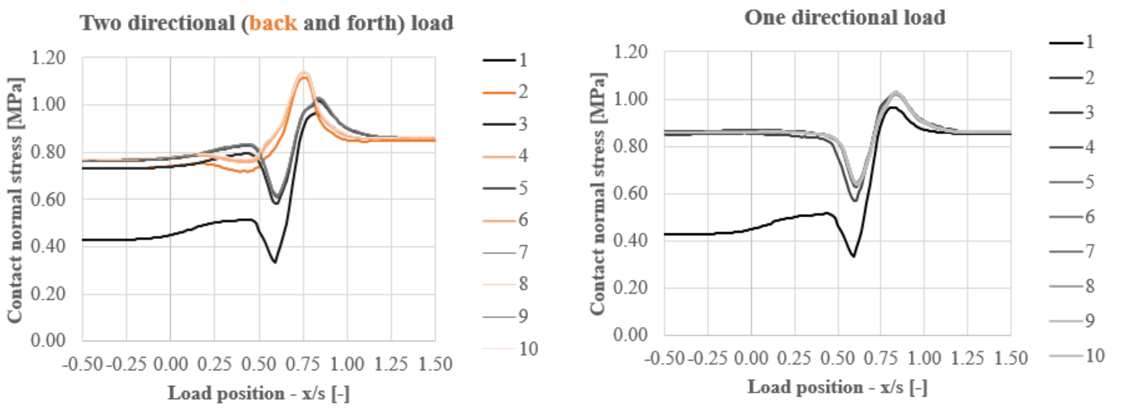

Figure 13 – Repeated loading (R_y=30 kN/m = 0.42 R_{ult}): influence lines for contact normal stress at ¾ span extrados: (a) two-directional; (b) one directional load path

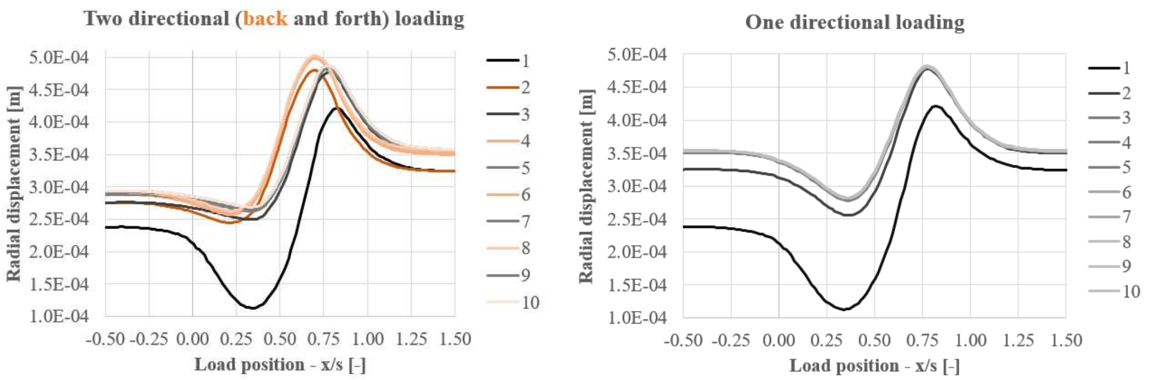

Figure 14 – Repeated loading (R_y = 30 kN/m = 0.42 R_{ult}): influence lines for radial displacements at ¾ span: (a) two-directional; (b) one directional load path

Simulations with repeated, one directional quasi-static loading were done with several external load magnitudes. If the magnitude of the external load does not exceed the ~50% of the ultimate load, then plastic deformations cease after 2-3 initial cycles and the response of the structure goes back to pure elastic with some state of residual stresses (Figure 15a-b). Similar shakedown phenomena was observed previously during the experimental test of masonry arches [44, 45]. Above ~50% of R_{ult} , additional plastic deformations were observed in every cycle of repeated loading. Also, at 85% of R_{ult}, equilibrium was not reached after the forth cycle which means that the structure has failed. It is worth to mention, that according to Figure 15a, the bridge which seemed to have sufficient resistance for $0.83R_{ult}$, collapsed after the forth cycle of loading with the same loading magnitude.

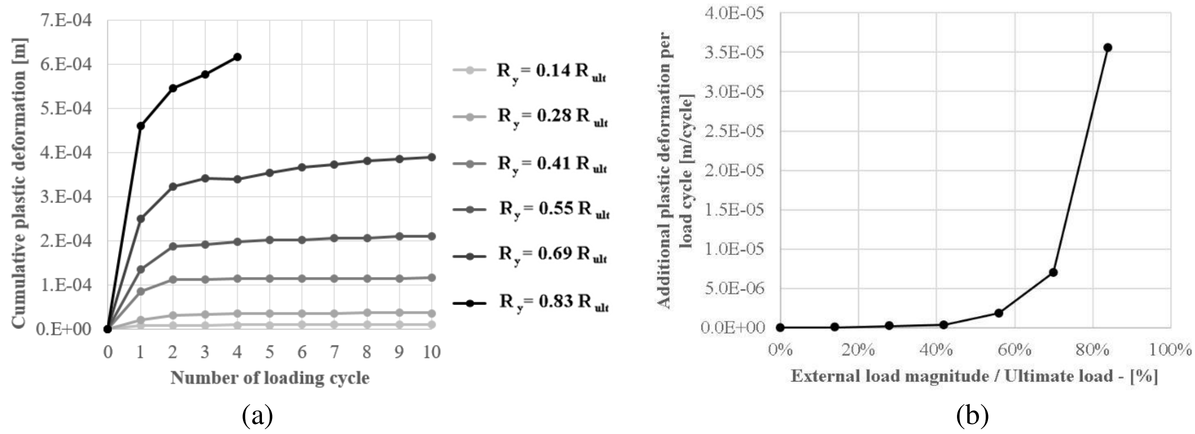

Figure 15 – Plastic shakedown of masonry arch bridge: (a) cumulative plastic deformation at ¾ span, (b) additional plastic deformations in a single load cycle

5.2. Results of dynamic analysis (Type 3)

In the dynamic analysis, the effect of vehicle-structure interaction was investigated. From the results analysis it was found that the vehicle-structure interaction is not significant i.e. the contact force between the track and the vehicle does not change significantly as the load passing through (Figure 16). This finding is in accordance with the EN 1991-2 and can be explained with significantly higher mass of the structure compared to the mass of the vehicle. As the magnitude of the external load gets closer to the ultimate load bearing capacity, the difference between the static and the dynamic contact force is increasing.

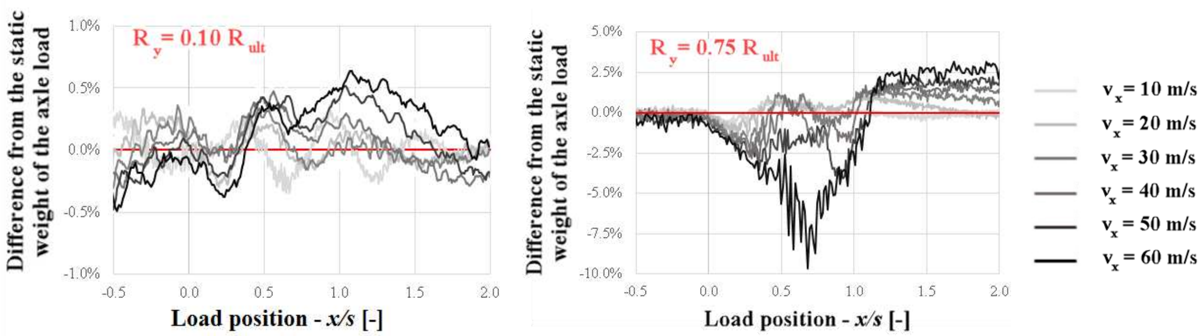

Figure 16 – Dynamic contact forces between the track and the vehicle

Also, as described in Section 4.3.3, dynamic analysis was carried out to obtain dynamic amplification factors and compared them with the multiplication factors calculated according to Network Rail standards. The investigated range of horizontal velocities was 10 m/s to 120 m/s. To decouple the phenomena of the plastic shakedown and the dynamic enhancement and exclude plastic deformations in the structure, all of the dynamic simulation was repeated 5 times, see Figure 17a-b. Moreover, influence lines for radial displacements at ¾ span (R_y =40 kN/m=0.55R_{ult}) were plotted and are shown in Figure 17b. As the velocity of the load increased and reached 100 m/s, radial displacements increased as well. On the other hand, for train speeds greater than 100 m/s, displacements in the structure decreased. The maximum response of the structure has a “delay” as the velocity increases compared to quasi-static analysis. The maximum value of outward (negative) radial displacement occurs when the load is at $x/s = 0.33$ in case of quasi-static analysis, while it is around $x/s = 0.55$ when the velocity is 120 m/s.

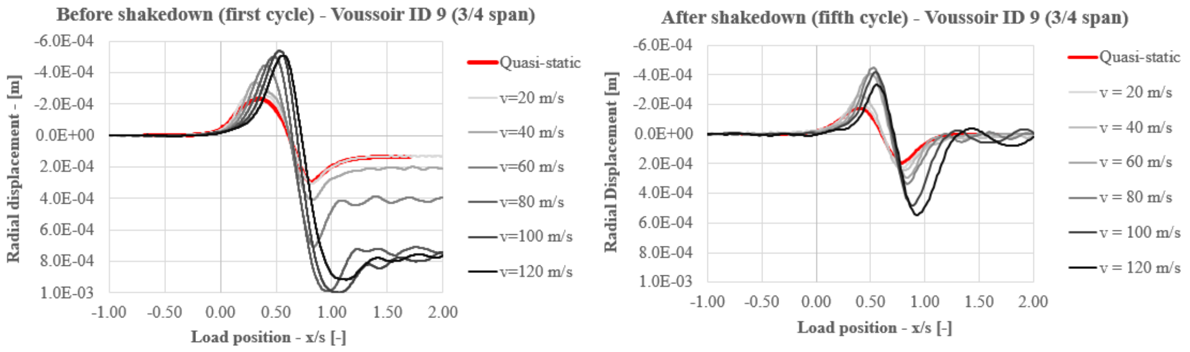

(a) (b)

Figure 17 – Influence lines for radial displacements at ¾ span (R_y =40 kN/m): (a) dynamic behaviour in the first loading cycle - before shakedown; (b) dynamic behaviour after shakedown

Radial displacement of every voussoir in the arch barrel was recorded and local dynamic amplification factors according to Eq (15) were calculated. From Figure 18 the DAF values are different at different parts of the arch barrel. The difference is increasing as the velocity of the external load is increasing. At Voussoir ID 1-8, significantly higher local DAFs were calculated. It should be noted, that the static response of the structure was very low at this part of the bridge.

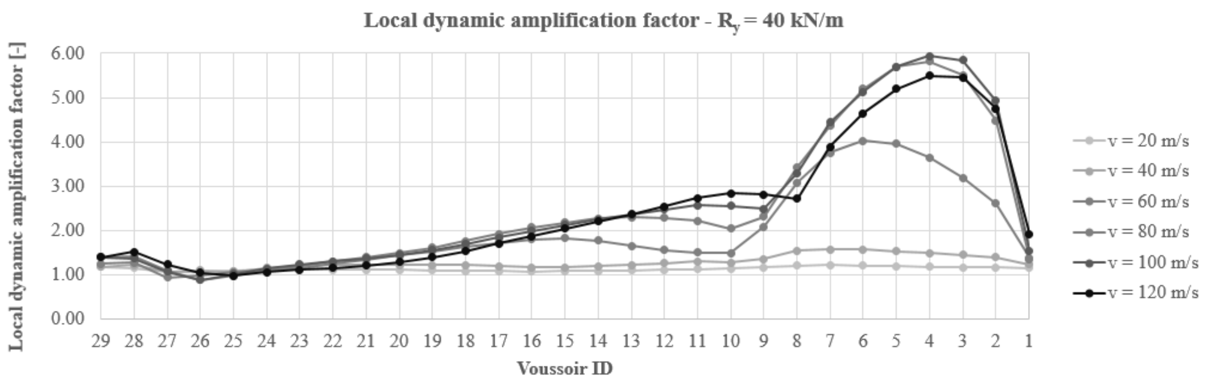

Figure 18- Local dynamic amplification factors for displacements at R_y = 40 kN/m

Dynamic amplification factors for displacements were calculated from Figure 17b and plotted in Figure 19. Moreover, simulations were repeated with different magnitude of external loads. The highest value of global DAF was around 210%. Critical speed – where the DAF has the highest value at a given magnitude of external load – is decreasing as the magnitude of the external load gets close to the ultimate load. Similarly, the highest value of DAF is slightly decreasing at higher level of external loads.

To compare the numerically obtained DAF with the ones given in guidelines, the natural frequency of the structure investigated in this work was determined with modal analysis. From the investigations, it was shown that the first natural frequency was ~30,5 Hz, which is between the limits of EN 1991-2 simplified method, hence the code is applicable $\Phi_2 = 1.67$ and $\Phi_3 = 2.00$. The dynamic enhancement according to the Network Rail standard (Eqs. 3 and 4) was calculated and shown in Figure 19. In the case of lower load levels (<40% R_{ult}), the formulas of the Network Rail provides a reasonably precise and safe estimate for DAFs. It should be noted, that if the external load is closer to the ultimate load bearing capacity, then the standard can underestimate the dynamic enhancement. From Figure 19 and Table 4, it is evident, that the critical speed (where the DAF value is the highest) is decreasing as the magnitude of the external load is increasing. This phenomena can be explained by the nonlinear behaviour of the structure: at higher load levels, the bridge starts to behave softer, hence the natural frequency of it is decreasing which is resulted in lower critical speeds.

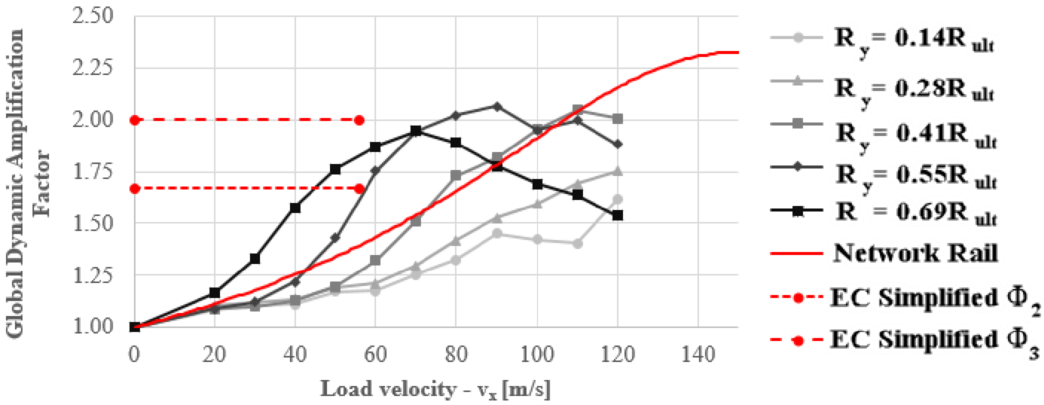

Figure 19 – Global Dynamic Amplification Factors for displacements at different level of external load

Table 4 – Critical speed at various load levels

External load level	Critical speed [m/s]
$0.14R_{ult}$	>120 m/s
$0.28R_{ult}$	>120 m/s
$0.41R_{ult}$	110 m/s
$0.55R_{ult}$	90 m/s
$0.69R_{ult}$	70 m/s

6. Conclusions

The structural assessment of masonry arch bridges is of great importance due to their long service life and deterioration condition over time. Dynamic amplification factor (DAF) is a parameter which accounts for the dynamic impact of moving trains on structures by relating the static to the dynamic characteristics of a bridge. Although, accurate prediction of the DAF can provide valuable information related to sustainable management of bridges, the structural assessment of the dynamic characteristics of masonry arch bridges and predictions of DAFs are rather difficult to be obtained. This is mainly due to the complexity of the problem and that recent studies have reported contradictory results. This paper focuses on the shakedown and dynamic behaviour of railway masonry arch bridges under traffic load conditions. A nonlinear, mixed discrete-finite element was developed to investigate the static and dynamic response of the Prestwood masonry arch bridge. Each voussoir of the masonry arch was represented by a distinct block. Mortar joints were modelled as zero thickness interfaces which can open and close depending on the magnitude and direction of the stresses applied to them. The numerical model was calibrated based on field full-scale experimental test results. The bridge was subjected to two different types of static analysis and a real dynamic analysis to simulate the effects of moving load. Investigations into the train to bridge interaction was also undertaken. Finally, the local and global Dynamic Amplification Factors were studied. The major findings of the work can be summarized as follows:

- Failure load of the investigated structure was determined in two different ways i.e. with monotonically increased loads at fixed positions and with quasi-static moving loads. From the results analysis it was shown that the latter reflects better the characteristic of real traffic since can take into account the interaction between the adjacent load positions. The load bearing capacity was 7% lower (71 kN/m) in case of "quasi-static moving load" type loading.
- As the external load passes through the bridge, plastic deformations and residual stresses exist in the arch barrel. If the magnitude of the external load does not exceed the 50% of the ultimate load bearing capacity, the plastic deformations cease after 2-3 cycles of external load and the structure is in a shakedown state. If the magnitude of the external load exceeds the 50% of the ultimate load, continuous plastic deformations were experienced in the loading cycles.
- With increasing load magnitude, the maximum contact normal stresses between the voussoirs are increasing exponentially.
- A single degree of freedom vehicle-structure interaction was developed and integrated within the developed code. Numerical experiences suggested, that vehicle-structure interaction has a negligible effect on the global behaviour of the bridge.
- Local and Global Dynamic Amplification Factors were introduced to have deeper insight into the dynamic enhancement. At different parts of the arch barrel, different magnitude of DAF was measured. It was shown that the dynamic amplification depends on the magnitude of the external load. As the load increases, non-linearity in the structural behaviour is evident, which decreases the natural frequency of the bridge. Hence the critical speed (i.e. where the highest DAF value can be measured) is decreasing.
- In the case of typical service load levels ($<40\%\ R_{ult}$), the formulas of the Network Rail provides a reasonably precise and safe estimate for DAFs. For this particular type of structure, for a service load greater than 40% R_{ult} the Network Rail formulas underestimate DAFs.

Limitation of the current work is that it neglects those structural element of a masonry bridge (e.g spandrel walls) which makes the structural behaviour three-dimensional. Moreover, further experimental studies will be needed to investigate the effect of geometry on the dynamic behaviour of masonry arch bridges to obtain more general results. Results presented from this study can improve understanding of the dynamic behaviour of masonry arch bridge and inform repair and maintenance schemes.

Acknowledgements

The authors express their gratitude to the ITASCA Education Partnership Program for providing a copy of UDEC software to assist the above research. The work presented in this paper was partially financially supported by an EPRSC doctoral training award (CASE/179/65/82).

References

[1] UIC. Code UIC 776-1R - Charges à Prendre en Considération Dans le Calcul des Ponts-Rails, 4e edition. 1994.

[2] Page JJ, Britain) TRLG. Masonry arch bridges: HMSO; 1993.

[3] Jensen JS, Casas JR, Karoumi R, Plos M, Cremona C, Melbourne C. Guideline for load and resistance assessment of existing european railway bridges. Fourth International Conference on Bridge Maintenance, Safety and Management (IABMAS 08). France2008. p. pp 3658-65.

[4] State of the Nation 2018: Infrastructure Investment. In: (ICE) IoCE, editor. UK: Institution of Civil Engineers (ICE); 2018. p. 31.

[5] Pippard AJS, Tranter E, Chitty L. The Mechanics of the Voussoir Arch. Journal of the Institution of Civil Engineers. 1936;4:281-306.

[6] Wang J, Haynes B, Melbourne C. A comparison between the MEXE and Pippard's methods of assessing the load carrying capacity of masonry arch bridges. ARCH'13 Proceedings of the 7th International Conference on Arch Bridges Trogir-Split, Croatia October 4-6, 2013: SECON-CSSE, Zagred, Croatia.; 2013. p. 589-96.

[7] Audenaert A, Beke J. Applicability analysis of 2D-models for masonry arch bridge assessment: Ring, Archie-M and the elasto-plastic model. WSEAS Transactions on applied and theoretical mechanics. 2010;5:221-30.

[8] Melbourne C, McKibbins L, Sawar N, Sicilia Gaillard C. Masonry arch bridges: condition appraisal and remedial treatment. London: University of Salford, UK; 2006.

[9] Fanning PJ, Boothby TE. Three-dimensional modelling and full-scale testing of stone arch bridges. Comput Struct. 2001;79:2645-62.

[10] Sarhosis V, De Santis S, de Felice G. A review of experimental investigations and assessment methods for masonry arch bridges. Structure and Infrastructure Engineering. 2016;12:1439-64.

[11] Choo BS, Gong NG. Effect of skew on the strength of masonry arch bridges. Arch Bridges. 1995:205-14.

[12] Giamundo V, Sarhosis V, Lignola GP, Sheng Y, Manfredi G. Evaluation of different computational modelling strategies for the analysis of low strength masonry structures. Engineering Structures. 2014;73:160-9.

[13] Boothby TE. Analysis of masonry arches and vaults. Progress in Structural Engineering and materials. 2001;3:246-56.

[14] Sarhosis V, Garrity SW, Sheng Y. Influence of brick-mortar interface on the mechanical behaviour of low bond strength masonry brickwork lintels. Engineering Structures. 2015;88:1-11.

[15] Moradabadi E, Laefer DF, Clarke JA, Lourenço PB. A semi-random field finite element method to predict the maximum eccentric compressive load for masonry prisms. Constr Build Mater. 2015;77:489-500.

[16] Lemos JV. Discrete Element Modeling of Masonry Structures. International Journal of Architectural Heritage. 2007;1:190-213.

[17] Zhang YY, Macorini L, Izzuddin BA. Numerical investigation of arches in brick-masonry bridges. Structure and Infrastructure Engineering. 2018;14:14-32.

[18] Forgács T, Sarhosis V, Bagi K. Influence of construction method on the load bearing capacity of skew masonry arches. Engineering Structures. 2018;168:612-27.

[19] Gago A, Alfaiate J, Gallardo A. Numerical analyses of the Bargower arch bridge. Finite elements in civil engineering applications Lisse (Tokyo): Swets & Zeitlinger. 2002.

[20] Ford T, Augarde C, Tuxford S. Modelling masonry arch bridges using commercial finite element software. 9th International Conference on Civil and Structural Engineering Computing, Egmond aan Zee, The Netherlands2003. p. 2-4.

[21] Drosopoulos G, Stavroulakis G, Massalas C. Limit analysis of a single span masonry bridge with unilateral frictional contact interfaces. Engineering Structures. 2006;28:1864-73.

[22] de Felice G. Assessment of the load-carrying capacity of multi-span masonry arch bridges using fibre beam elements. Engineering Structures. 2009;31:1634-47.
[23] De Santis S, de Felice G. A fibre beam-based approach for the evaluation of the seismic capacity of masonry arches. Earthq Eng Struct D. 2014;43:1661-81.
[24] Cundall PA. A computer model for simulating progressive, large-scale movements in blocky rock systems. Proc Int Symp on Rock Fracture. 1971:11-8.
[25] Mirabella R, Calvetti E. Distinct element analysis of stone arches. Sinopoli (ed), Arch Bridges; Proc Intern Symp, Paris1998. p. 6-9.
[26] Toth AR, Orban Z, Bagi K. Discrete element analysis of a stone masonry arch. Mech Res Commun. 2009;36:469-80.
[27] Sarhosis V, Sheng Y. Identification of material parameters for low bond strength masonry. Engineering Structures. 2014;60:100-10.
[28] Eurocode 1: Actions on structures–Part 2: Traffic loads on bridges. 2003.
[29] Rail N. The structural assessment of underbridges. Network Rail, London, UK, Guidance Note NR/GN/CIV/025. 2006.
[30] Smith J, Acikgoz S. Dynamic Amplification of Curved Beams Subjected to a Moving Point Load. 2020. p. 212-20.
[31] Costa C, Arêde A, Costa A. Numerical simulation of stone masonry arch bridges behaviour under road traffic moving loads. Proceedings of ARCH'10-the 6~(th) International Conference on Arch Bridges2010.
[32] Jorge P, Ribeiro D, Costa C, Arêde A, Calçada R. Train-bridge dynamic interaction on a stone masonry railway bridge2016.
[33] Silva R, Costa C, Arêde A. Nonlinear Analysis of a Multispan Stone Masonry Bridge Under Railway Traffic Loading. International Conference on Arch Bridges: Springer; 2019. p. 119-27.
[34] Rafiee-Dehkharghani R, Ghyasvand S, Sahebalzamani P. Dynamic Behavior of Masonry Arch Bridge under High-Speed Train Loading: Veresk Bridge Case Study. J Perform Constr Fac. 2018;32:04018016.
[35] Ataei S, Miri A. Investigating dynamic amplification factor of railway masonry arch bridges through dynamic load tests. Constr Build Mater. 2018;183:693-705.
[36] D214/RP9 E. Railway bridges for speeds> 200 km/h. European Rail Research Institute (ERRI) Utrecht; 2001.
[37] Ladislav F. Dynamics of Railway Bridges. 1996.
[38] ITASCA. UDEC - Universal Distinct Element Code Manual. Theory and Background. Mineapolis, USA: Itasca Consulting Group; 2004.
[39] Sarhosis V, Forgács T, Lemos JV. A discrete approach for modelling backfill material in masonry arch bridges. Comput Struct. 2019;224:106108.
[40] Forgacs T, Sarhosis V, Ádány S. Discrete Element Modeling of skew masonry arch bridges taking into account arch ring-backfill interaction. In: Milani G, Taliercio A, Garrity S, editors. 10th International Masonry Conference. Milan, Italy2018.
[41] Forgács T, Rendes S, Ádány S, Sarhosis V. Mechanical Role of Spandrel Walls on the Capacity of Masonry Arch Bridges. International Conference on Arch Bridges: Springer; 2019. p. 221-9.
[42] Page J. Load tests to collapse on two arch bridges at Preston, Shropshire and Prestwood, Staffordshire. 1987.
[43] Marti J, Cundall P. Mixed discretization procedure for accurate modelling of plastic collapse. Int J Numer Anal Met. 1982;6:129-39.
[44] Rosson BT, Søyland K, Boothby TE. Inelastic behavior of sand-lime mortar joint masonry arches. Engineering structures. 1998;20:14-24.
[45] Boothby TE, Rosson BT. Elasto-plastic Hardening and Shakedown of Masonry Arch Joints. Meccanica. 1999;34:71-84.